A Novel Second-order Scheme for the Molecular Beam Epitaxy Model with Slope Selection

Lizhen Chen[1], Jia Zhao[2,*], and Yuezheng Gong[3]

[1] *Beijing Computational Science Research Center, Beijing, P.R. China*
[2] *Utah State University, Logan, UT, USA*
[3] *College of Science, Nanjing University of Aeronautics and Astronautics, Nanjing 210016, P.R. China*

Abstract. Molecular beam epitaxy (MBE) is a very important and challenging research topic in material science. In this paper, we focus on a well-celebrated continuum MBE model. Namely, we propose a new fully discrete scheme for the MBE model with slope selection. First of all, we use a multi-step strategy to discretize the MBE model in time. The obtained semi-discrete second-order scheme is proved to possess total mass conservation, unconditionally energy stability and uniquely solvability. The rigorous error estimate is then conducted to show its second-order convergence. The semi-discrete scheme is further discretized in space using the Fourier pseudospectral method. The fully discrete scheme is also shown to preserve mass-conservation and energy-dissipation properties. Afterward, several numerical examples are presented to validate the accuracy and efficiency of our proposed scheme. In particular, the scaling law for the roughness growing and effective energy decaying are captured during long-time coarsening dynamic simulations. The idea proposed in this paper could be readily utilized to design accurate and stable numerical approximations for many other energy-based phase field models.

1 Introduction

Molecular beam epitaxy (MBE) method is a broadly used approach of thin-film deposition of a single crystal. And this strategy is widely applied in semiconductor manufacture. In recent years, MBE becomes a very important and challenging research topic in material science. In the meanwhile, many mathematical models have been developed to study the epitaxy dynamics, ranging from molecular dynamics simulations to continuum models [1, 6, 11, 15, 17, 19, 22, 23, 28, 31].

In this paper, we focus on one broadly-used continuum model for the MBE, which is derived via an energy variational approach and satisfies an energy dissipation law (i.e.,

*Corresponding author. *Email addresses:* lzchen@csrc.ac.cn. (L. Chen), jia.zhao@usu.edu. (J. Zhao), gongyuezheng@nuaa.edu.cn. (Y. Gong)

thermodynamically consistent) [22, 23, 33, 35]. Consider a smooth domain Ω, and use $\phi(\mathbf{x},t):\Omega\to\mathbb{R}$ to denote the height function of MBE, and the effective free energy is given as

$$E(\phi)=\int_\Omega\Big[\frac{\varepsilon^2}{2}|\Delta\phi|^2+f(\nabla\phi)\Big]d\Omega. \tag{1.1}$$

Here the first term represents the isotropic surface diffusion effect, and the second term approximates the Enrlich-Schwoebel effect that the adatoms stick to the boundary from an upper terrace, contributing to the steepening of mounds in the film [3]. The evolution equation for ϕ could be derived via a L^2 gradient flow associated with the effective free energy functional $E(\phi)$, i.e., the equation reads as

$$\partial_t\phi=-M\frac{\delta E}{\delta\phi}, \tag{1.2}$$

where M is the mobility parameter (with $\frac{1}{M}$ proportional to the relaxation time). For simplicity of notations, we consider periodic boundary condition in this paper.

If we choose the second term as $f(\nabla\phi)=-\frac{1}{2}\ln(1+|\nabla\phi|^2)$, the corresponding equation would be

$$\partial_t\phi=-M\Big(\varepsilon^2\Delta^2\phi+\nabla\cdot(\frac{\nabla\phi}{1+|\nabla\phi|^2})\Big), \tag{1.3}$$

and its energy dissipation rate could be calculated as

$$\frac{dE}{dt}=-\int_\Omega M\Big(\varepsilon^2\Delta^2\phi+\nabla\cdot(\frac{\nabla\phi}{1+|\nabla\phi|^2})\Big)^2d\Omega. \tag{1.4}$$

On the other hand, if we choose $f(\nabla\phi)=\frac{1}{4}(|\nabla\phi|^2-1)^2$, the corresponding equation would become

$$\partial_t\phi=-M\Big(\varepsilon^2\Delta^2\phi+\nabla\cdot((1-|\nabla\phi|^2)\nabla\phi)\Big), \tag{1.5}$$

and its energy dissipation rate could be calculated as

$$\frac{dE}{dt}=-\int_\Omega M\Big(\varepsilon^2\Delta^2\phi+\nabla\cdot((1-|\nabla\phi|^2)\nabla\phi)\Big)^2d\Omega. \tag{1.6}$$

In addition, both models (1.3) and (1.5) obey the total mass conservation law

$$\frac{d}{dt}\int_\Omega\phi(\mathbf{x},t)d\Omega=0. \tag{1.7}$$

Notice when the surface gradient $|\nabla\phi|$ is small ($|\nabla\phi|<<1$), by Taylor expansion, we can easily recognize $\frac{1}{1+|\nabla\phi|^2}\approx 1-|\nabla\phi|^2$. Then model (1.5) could be formally derived from model (1.3). These two models (1.3) and (1.5) have been extensively applied to study coarsening dynamics in molecular beam epitaxial growth. The model (1.5) is usually named "MBE model with slope section", as it has a slope selection preference, i.e., $|\nabla\phi|=$

1 is preferred. Correspondingly, the model (1.3) is usually named "MBE model without slope selection".

Another view for the two models (1.3) and (1.5) is through conservation of mass. By Fick's first law, we have

$$\partial_t \phi + \nabla \cdot \mathbf{J} = 0, \tag{1.8}$$

where $\mathbf{J}$ is the surface current depending on the macroscopic gradient $\nabla\phi$ of the film surface. For model (1.3), the flux is

$$\mathbf{J} = M\left(\varepsilon^2 \nabla \Delta \phi + \frac{1}{1+|\nabla\phi|^2}\nabla\phi\right), \tag{1.9}$$

with the first term representing the isotropic surface diffusion due to the surface tension, and the second term representing the kinetic surface current due to the Ehrlich-Schwoebel effect. Similarly, for model (1.5), the flux is given as

$$\mathbf{J} = M\left(\varepsilon^2 \nabla \Delta \phi + (1-|\nabla\phi|^2)\nabla\phi\right). \tag{1.10}$$

We can easily see the difference between the two models (1.3) and (1.5) lies in the different approximation of Ehrlich-Schwoebel effect.

The two models (1.3) and (1.5) have been intensively investigated both analytically and numerically [2, 3, 9, 10, 16, 18, 21, 22, 25, 26, 29, 30, 32, 34, 35]. Define the roughness $W(t) = \sqrt{\frac{1}{|\Omega|}\int_\Omega (\phi(\mathbf{x},t)-\overline{\phi})^2 d\Omega}$, which is the standard deviation of the height profile. It is shown that the scaling law is $W(t) \sim t^{\frac{1}{2}}$ for the MBE model without slope section (1.3). In the meanwhile, for the MBE model with slope selection (1.5), the roughness $W(t)$ grows like $O(t^{\frac{1}{3}})$ and the energy $E(t)$ decays like $O(t^{-\frac{1}{3}})$ [21]. Thus in order to reach steady state, designing accurate and stable numerical schemes, for the MBE models for conducting long-time dynamic simulations, are essential. A great amount of work have been published in designing numerical schemes for the MBE models, including unconditionally energy stable schemes using convex splitting method [29, 32], adaptive in time method [27], operator splitting strategy [5, 20], invariant energy-quantization (IEQ) approach [2, 35], SAV approach [30] etc. Error analysis have also been conducted [2,4,10,24–26]. The operator splitting strategy is very efficient, but lacks theoretical foundations. The convex splitting schemes are shown to be uniquely solvable and unconditionally energy stable, but at each time step a nonlinear system has to be solved. The IEQ approach and SAV approach provide uniquely solvable linear schemes,which however based on a modified free energy functional.

In this paper, we add to these available numerical schemes with a new one. Inspired by the framework in [7], we propose a multi-step method for solving the MBE model with slope selection. The inspiring work in [7] provides an elegant approach for developing conservative numerical integrators for dispersive partial differential equations with polynomial nonlinearities. We are able to apply it for the MBE model with slope

selection. Our newly proposed numerical scheme is linear, such that only a linear algebra problem needs to be solved at every time marching step. The scheme is second-order in time and proven to be unconditionally energy stable and uniquely solvable, such that large time step is durable for long-time dynamic simulation. To our best knowledge, this efficient and accurate multi-step scheme for the MBE model has never been studied. Thus, the results in this paper provide a new contribution to the numerical analysis of MBE models.

The rest of the paper is organized as follows. In Section 2, we develop the numerical schemes and prove their unconditional energy stability, unique solvability and error estimate in the semi-discretized case in time. In Section 3, we present some numerical simulations to demonstrate the accuracy and efficiency of the proposed schemes. Finally, some concluding remarks are presented in Section 3.3.

2 Numerical Schemes

Here we briefly recall the MBE model with slope selection and present the numerical schemes afterward. Denote Ω the computational domain. Let ϕ represents the epitaxy surface height, ε be a model parameter controlling the strength of surface diffusion, and M be the mobility coefficient. The MBE model reads

$$\begin{cases} \partial_t \phi(\mathbf{x},t) = -M\Big(\varepsilon^2\Delta^2\phi - \nabla\cdot((|\nabla\phi|^2-1)\nabla\phi)\Big), \quad (\mathbf{x},t)\in\Omega\times(0,T] \\ \phi(\mathbf{x},0) = \phi_0, \quad \mathbf{x}\in\Omega, \end{cases} \tag{2.1}$$

with the periodic boundary condition or any other proper boundary condition that can satisfy the flux free condition at the boundary $\partial_{\mathbf{n}}\phi|_{\partial\Omega}=0$ and $\partial_{\mathbf{n}}\Delta\phi|_{\partial\Omega}=0$, where $\mathbf{n}$ is the outward normal on the boundary.

The model (2.1) has two major properties. First of all, we can easily obtain the mass conservation property

$$\frac{d}{dt}\int_\Omega \phi(\mathbf{x},t)d\Omega = 0. \tag{2.2}$$

Secondly, the model is thermodynamically consistent in the sense that its energy is dissipative in time. As a matter of fact, the energy dissipation rate could be calculated as

$$\frac{dE(t)}{dt} = \int_\Omega \Big(\frac{\delta E}{\delta\phi}\frac{\delta\phi}{\delta t}\Big)d\Omega = -\int_\Omega M\Big(\varepsilon^2\Delta^2\phi - \nabla\cdot((|\nabla\phi|^2-1)\nabla\phi)\Big)^2 d\Omega. \tag{2.3}$$

Thus, we would like to propose an accurate and efficient discrete numerical scheme to preserve the properties: (1) mass conservation; (2) energy dissipation. So the results calculated via the discrete numerical scheme would be physically consistent. Such kinds of numerical schemes that preserve the non-negative energy dissipation laws are unusually named energy stable numerical approximations [8, 13, 14, 36, 37].

2.1 The new Multi-step Crank-Nicolson scheme

Next, we propose the semi-discrete numerical approximations to the MBE model (2.1). For simplicity of notation, we assume periodic boundary condition. Here we present a second-order in time, unconditionally energy stable scheme based on a multi-step Crank-Nicolson time discretization approach. The temporal semi-discrete scheme reads

Scheme 2.1. *Given the initial condition $\phi^0=\phi_0$, we calculate ϕ^1 via a first order time marching scheme with smaller time steps, such that ϕ^1 is second-order accurate in term of δt. For instance, we update $\phi^1=\tilde{\phi}^1_N$, where*

$$\frac{\tilde{\phi}^1_{i+1}-\tilde{\phi}^1_i}{\delta t^1}=-M\Big[\varepsilon^2\Delta^2\tilde{\phi}^1_{i+1}-\nabla\cdot(|\nabla\tilde{\phi}^1_i|^2\nabla\tilde{\phi}^1_{i+1})+\Delta\tilde{\phi}^1_{i+1}\Big],i=0,1,\cdots,N-1, \tag{2.4}$$

with $\delta t^1=\frac{\delta t}{[\frac{1}{\delta t}+1]}$, $N=[\frac{1}{\delta t}+1]$ and $\tilde{\phi}^1_0=\phi^0$. After we obtained ϕ^n,ϕ^{n+1} , $\forall n\geq 0$, we update ϕ^{n+2} via

$$\begin{aligned}\frac{\phi^{n+2}-\phi^n}{2\delta t} &= -M\Big[\varepsilon^2\Delta^2\frac{\phi^{n+2}+\phi^n}{2}-\nabla\cdot\Big(|\nabla\phi^{n+1}|^2\nabla\frac{\phi^{n+2}+\phi^n}{2}\Big)\\ &\quad -\gamma\Delta\frac{\phi^{n+2}+\phi^n}{2}+(1+\gamma)\Delta\phi^{n+1}\Big],\end{aligned} \tag{2.5}$$

where $\gamma\geq 0$ is a regularization parameter.

Theorem 2.1. *Under the periodic boundary condition, Scheme 2.1 possesses the discrete mass conservation law*

$$(\phi^n,1)=(\phi^0,1),\quad \forall n\geq 0.$$

Proof. Computing the inner product of Eq. (2.5) with $2\delta t$ and using some proper integration formulas, we have

$$(\phi^{n+2},1)=(\phi^n,1),\quad \forall n\geq 0. \tag{2.6}$$

Similarly, we can deduce from (2.4)

$$(\phi^1,1)=(\phi^0,1). \tag{2.7}$$

Therefore, it holds

$$(\phi^n,1)=(\phi^0,1),\quad \forall n\geq 0. \tag{2.8}$$

□

Theorem 2.2. *For Scheme 2.1, there exists a unique solution $\phi^{n+2}\in H^2_{per}(\Omega)$, $\forall n\geq 0$.*

Proof. First of all, let us look at the Scheme 2.1. For any $n\geq 0$, it is equivalent to solve a linear system

$$\mathcal{T}\phi=f, \tag{2.9}$$

where the linear operator $\mathcal{T}$ and right-hand-side f are given as

$$\begin{aligned}\mathcal{T}\phi &= \frac{1}{2\delta t}\phi + M\Big[\frac{\varepsilon^2}{2}\Delta^2\phi - \frac{1}{2}\nabla\cdot(|\nabla\phi^{n+1}|^2\nabla\phi) - \frac{\gamma}{2}\Delta\phi\Big],\\ f &= \frac{1}{2\delta t}\phi^n - M\Big[\frac{\varepsilon^2}{2}\Delta^2\phi^n - \frac{1}{2}\nabla\cdot(|\nabla\phi^{n+1}|^2\nabla\phi^n) - \frac{\gamma}{2}\Delta\phi^n + (1+\gamma)\Delta\phi^{n+1}\Big].\end{aligned}$$

Then the weak form of (2.9) reads as, find $\phi \in H^2_{per}(\Omega)$ such that

$$a(\phi,\psi) = f(\psi), \quad \forall \psi \in H^2_{per}(\Omega), \tag{2.10}$$

where $\phi^n, \phi^{n+1} \in H^2_{per}(\Omega)$ and

$$\begin{aligned}&a(\phi,\psi) = \frac{1}{2\delta t}(\phi,\psi) + \frac{M\varepsilon^2}{2}(\Delta\phi,\Delta\psi) + \frac{M}{2}(|\nabla\phi^{n+1}|^2\nabla\phi,\nabla\psi) + \frac{M\gamma}{2}(\nabla\phi,\nabla\psi),\\ &f(\psi) = (f,\psi).\end{aligned}$$

It could be easily verified that the bilinear form $a(\cdot,\cdot)$ is continuous and coercive, and the linear form f is continous. Using the Lax-Milgram theorem, we obtain that there exists a unique solution $\phi^{n+2} \in H^2_{per}(\Omega)$ in (2.10) , for all $n \geq 0$. This completes the proof. □

Theorem 2.3. *Under the periodic boundary condition, Scheme 2.1 satisfies the following discrete energy dissipation law*

$$\frac{E[\phi^{n+1},\phi^{n+2}] - E[\phi^n,\phi^{n+1}]}{\delta t} = -\frac{1}{M}\left\|\frac{\phi^{n+2}-\phi^n}{2\delta t}\right\|^2, \quad \forall n \geq 0, \tag{2.11}$$

where the discrete free energy is defined as

$$\begin{aligned}E[\phi^n,\phi^{n+1}] &= \frac{\varepsilon^2}{4}(\|\Delta\phi^n\|^2 + \|\Delta\phi^{n+1}\|^2) + \frac{1}{4}(|\nabla\phi^n|^2, |\nabla\phi^{n+1}|^2)\\ &\quad + \frac{\gamma}{4}(\|\nabla\phi^n\|^2 + \|\nabla\phi^{n+1}\|^2) - \frac{1+\gamma}{2}(\nabla\phi^n,\nabla\phi^{n+1}) + (\frac{1}{4},1).\end{aligned}$$

Proof. By a straightforward calculation, we have

$$\begin{aligned}
& E[\phi^{n+1},\phi^{n+2}]-E[\phi^n,\phi^{n+1}] \\
= \;& \frac{\varepsilon^2}{4}(\|\Delta\phi^{n+2}\|^2-\|\Delta\phi^n\|^2)+\frac{1}{4}(|\nabla\phi^{n+2}|^2-|\nabla\phi^n|^2,|\nabla\phi^{n+1}|^2) \\
& +\frac{\gamma}{4}(\|\nabla\phi^{n+2}\|^2-\|\nabla\phi^n\|^2)-\frac{1+\gamma}{2}(\nabla\phi^{n+2}-\nabla\phi^n,\nabla\phi^{n+1}) \\
= \;& \frac{\varepsilon^2}{4}\Big(\Delta(\phi^{n+2}+\phi^n),\Delta(\phi^{n+2}-\phi^n)\Big)+\frac{1}{4}\Big(|\nabla\phi^{n+1}|^2\nabla(\phi^{n+2}+\phi^n),\nabla(\phi^{n+2}-\phi^n)\Big) \\
& +\frac{\gamma}{4}\Big(\nabla(\phi^{n+2}+\phi^n),\nabla(\phi^{n+2}-\phi^n)\Big)-\frac{1+\gamma}{2}\Big(\nabla\phi^{n+1},\nabla(\phi^{n+2}-\phi^n)\Big) \\
= \;& \frac{\varepsilon^2}{4}\Big(\Delta^2(\phi^{n+2}+\phi^n),\phi^{n+2}-\phi^n\Big)-\frac{1}{4}\Big(\nabla\cdot(|\nabla\phi^{n+1}|^2\nabla(\phi^{n+2}+\phi^n)),\phi^{n+2}-\phi^n\Big) \\
& -\frac{\gamma}{4}\Big(\Delta(\phi^{n+2}+\phi^n),\phi^{n+2}-\phi^n\Big)+\frac{1+\gamma}{2}\Big(\Delta\phi^{n+1},\phi^{n+2}-\phi^n\Big) \\
= \;& \delta t\Big(\varepsilon^2\Delta^2\frac{\phi^{n+2}+\phi^n}{2}-\nabla\cdot(|\nabla\phi^{n+1}|^2\nabla\frac{\phi^{n+2}+\phi^n}{2})-\gamma\Delta\frac{\phi^{n+2}+\phi^n}{2}+(1+\gamma)\Delta\phi^{n+1},\frac{\phi^{n+2}-\phi^n}{2\delta t}\Big) \\
= \;& -\frac{\delta t}{M}\left\|\frac{\phi^{n+2}-\phi^n}{2\delta t}\right\|^2,
\end{aligned}$$

where some integration formulas and Eq. (2.5) are used. This completes the proof. □

Remark 2.1. It could be easily seen that $E[\phi^n,\phi^{n+1}]$ (for all $n\geq 0$) is bounded from below, by noticing the fact

$$\frac{1}{4}|\nabla\phi^n|^2|\nabla\phi^{n+1}|^2-\frac{1}{2}\nabla\phi^n\cdot\nabla\phi^{n+1}+\frac{1}{4}\geq\frac{1}{4}\Big(\nabla\phi^n\cdot\nabla\phi^{n+1}-1\Big)^2\geq 0, \tag{2.12}$$

and

$$\frac{\gamma}{4}(|\nabla\phi^n|^2+|\nabla\phi^{n+1}|^2)-\frac{\gamma}{2}\nabla\phi^n\cdot\nabla\phi^{n+1}=\frac{\gamma}{4}\Big|\nabla\phi^n-\nabla\phi^{n+1}\Big|^2\geq 0,\quad\forall\gamma\geq 0. \tag{2.13}$$

2.2 Error analysis

To simplify the notations, we let $M=\varepsilon=1$ in the below without loss of generality. We use $x\lesssim y$ to denote there exists a constant C that is independent of δt and n such that $x\leq Cy$. Denote $L^p(\Omega)$ be the usual Lebesgue space on Ω with the norm $\|\cdot\|_{L^p}$. The inner product and norm in $L^2(\Omega)$ are denoted by $(\cdot,\cdot)$ and $\|\cdot\|$, respectively. $W^{k,p}(\Omega)$ stands for the standard Sobolev spaces equipped with the standard Sobolev norms $\|\cdot\|_{k,p}$. For $p=2$, we write $H^k(\Omega)$ for $W^{k,2}(\Omega)$, and the corresponding norm is $\|\cdot\|_k$.

Now we begin to derive the error estimates for the Scheme 2.1. We formulate the

model (2.1) as a truncation form:

$$\begin{aligned}\frac{\phi(t_{n+2})-\phi(t_n)}{2\delta t}=&-\Big[\Delta^2\frac{\phi(t_{n+2})+\phi(t_n)}{2}-\gamma\Delta\frac{\phi(t_{n+2})+\phi(t_n)}{2}\\&+(1+\gamma)\Delta\phi(t_{n+1})-\nabla\cdot(|\nabla\phi(t_{n+1})|^2\nabla\frac{\phi(t_{n+2})+\phi(t_n)}{2})\Big]+R^{n+1},\end{aligned}\tag{2.14}$$

where

$$\begin{aligned}R^{n+1}\quad=&\frac{\phi(t_{n+2})-\phi(t_n)}{2\delta t}-\phi_t(t_{n+1})+\Delta^2\frac{\phi(t_{n+2})+\phi(t_n)}{2}-\Delta^2\phi(t_{n+1})\\&-\gamma\Delta\frac{\phi(t_{n+2})+\phi(t_n)}{2}+\gamma\phi(t_{n+1})-\nabla\cdot(|\nabla\phi(t_{n+1})|^2\nabla\frac{\phi(t_{n+2})+\phi(t_n)}{2})\\&+\nabla\cdot(|\nabla\phi(t_{n+1})|^2\nabla\phi(t_{n+1})).\end{aligned}$$

We assume the exact solution ϕ of the system (2.1) possesses the following regularity conditions

$$\phi\in L^\infty(0,T;H^2(\Omega)),\phi_t\in L^2(0,T;L^2(\Omega))\cap L^\infty(0,T;H^2(\Omega)),\phi_{tt}\in L^2(0,T;L^2(\Omega)).\tag{2.15}$$

Lemma 2.1. *Under the regularity conditions* (2.15)*, the truncation errors satisfy*

$$\delta t\sum_{n=0}^{[\frac{T}{\delta t}]}\|R^{n+1}\|^2\lesssim\delta t^4.$$

The proof of Lemma 2.1 is straight forward by the Taylor expression and thus is omitted here.

Lemma 2.2. *The numerical solution ϕ^{n+1}, $\forall n\geq 0$ from Scheme 2.1 has an $H^2_{per}(\Omega)$ bound, thus is $L^\infty_{per}(\Omega)$ bounded.*

Proof. From (2.11), there exists a constant C such that

$$\|\Delta\phi^{n+1}\|_0^2+\|\nabla\phi^{n+1}\|_0^2\lesssim E(\phi^{n+1},\phi^n)\leq E(\phi^1,\phi^0)\leq C.$$

Noticing the mass conservation $\int_\Omega\phi^{n+1}d\Omega=$ constant, we have $\phi^{n+1}\in H^2_{per}(\Omega),\forall n\geq 0$. Then by the Sobolev inequality

$$\|\phi^{n+1}\|_\infty\leq C_\Omega\|\phi^{n+1}\|_1^{\frac{1}{2}}\|\phi^{n+1}\|_2^{\frac{1}{2}},$$

where C_Ω is a constant that only depends on Ω. This means that $\phi^{n+1}\in L^\infty_{per}(\Omega),\forall n\geq 0$. □

Remark 2.2. Notice that the energy stability is in terms of a numerically modified energy functional. For the original energy functional, one could derive its bound after the H^2

bound becomes available, as given by Lemma 2.2; meanwhile, an ε-independent bound for the original energy functional is not theoretically available.

To derive the error estimates, we denote the error functions as

$$e^n = \phi(t_n) - \phi^n. \tag{2.16}$$

By subtracting (2.14) from (2.5), we derive the error equations:

$$\begin{aligned} &\frac{e^{n+2}-e^n}{2\delta t} + \Delta^2 \frac{e^{n+2}+e^n}{2} - \gamma\Delta \frac{e^{n+2}+e^n}{2} + (1+\gamma)\Delta e^{n+1} \\ &= \nabla\cdot(|\nabla\phi(t_{n+1})|^2 \nabla \frac{e^{n+2}+e^n}{2}) \\ &+ \nabla\cdot((|\nabla\phi(t_{n+1})|^2 - |\nabla\phi^{n+1}|^2)\nabla\frac{\phi^{n+2}+\phi^n}{2}) + R^{n+1}. \end{aligned} \tag{2.17}$$

Theorem 2.4. *Under the regularity conditions of* (2.15)*, for* $0 \le m \le [\frac{T}{\delta t}] - 1$*, it holds*

$$\|\Delta e^{m+1}\|^2 + \gamma\|\nabla e^{m+1}\|^2 \lesssim \delta t^4. \tag{2.18}$$

Proof. Here we present the proof by induction. Given $\|\Delta e^k\|^2 + \gamma\|\nabla e^k\|^2 \lesssim \delta t^4$, $\forall k \le m$, we are going to show $\|\Delta e^{m+1}\|^2 + \gamma\|\nabla e^{m+1}\|^2 \lesssim \delta t^4$.

By taking the L^2 inner product of (2.17) with $2\delta t(e^{n+2}-e^n)$, we obtain

$$\begin{aligned} \|e^{n+2}-e^n\|^2 \quad &+\delta t\Big(\|\Delta e^{n+2}\|^2 - \|\Delta e^n\|^2\Big) + \gamma\delta t\Big(\|\nabla e^{n+2}\|^2 - \|\nabla e^n\|^2\Big) \\ &= 2(1+\gamma)\delta t(\nabla e^{n+1}, \nabla(e^{n+2}-e^n)) \\ &-\delta t(|\nabla\phi(t_{n+1})|^2\nabla(e^{n+2}+e^n), \nabla(e^{n+2}-e^n)) \\ &-\delta t\Big((|\nabla\phi(t_{n+1})|^2 - |\nabla\phi^{n+1}|^2)\nabla(\phi^{n+2}+\phi^n), \nabla(e^{n+2}-e^n)\Big) \\ &+2\delta t(R^{n+1}, e^{n+2}-e^n). \end{aligned}$$

We estimate the terms on the right hand side one by one as follows. For the first term, we have

$$2(1+\gamma)\delta t(\nabla e^{n+1}, \nabla(e^{n+2}-e^n)) \lesssim \delta t^2\|\Delta e^{n+1}\|^2 + \frac{1}{4}\|e^{n+2}-e^n\|^2, \tag{2.19}$$

and for the second term, we have

$$\begin{aligned} &-\delta t(|\nabla\phi(t_{n+1})|^2\nabla(e^{n+2}+e^n), \nabla(e^{n+2}-e^n)) \\ &\lesssim \delta t^2(\|\triangle e^{n+2}\|^2 + \|\triangle e^n\|^2 + \|\nabla e^{n+2}\|^2 + \|\nabla e^n\|^2) + \frac{1}{4}\|e^{n+2}-e^n\|^2. \end{aligned} \tag{2.20}$$

Notice that the fact

$$\begin{aligned} & |(\nabla\phi(t_{n+1}))^2-(\nabla\phi^{n+1})^2| \\ \leq\ & |\nabla\phi(t_{n+1})-\nabla\phi^{n+1}||\nabla\phi^{n+1}+\nabla\phi(t_{n+1})| \\ =\ & |\nabla\phi(t_{n+1})-\nabla\phi^{n+1}||\nabla\phi^{n+1}-\nabla\phi(t_{n+1})+2\nabla\phi(t_{n+1})| \\ \lesssim\ & |\nabla e^{n+1}|\lesssim\delta t^2, \end{aligned} \tag{2.21}$$

by acknowledging Lemma 2.2. Then for the third term, we have

$$\begin{aligned} & -\delta t((|\nabla\phi(t_{n+1})|^2-|\nabla\phi^{n+1}|^2)\nabla(\phi^{n+2}+\phi^n)),\nabla(e^{n+2}-e^n)) \\ & -\delta t((|\nabla\phi(t_{n+1})|^2-|\nabla\phi^{n+1}|^2)\nabla(e^{n+2}+e^n+\phi(t_{n+2})+\phi(t_n))),\nabla(e^{n+2}-e^n)) \\ & \lesssim\delta t^3(\nabla|e^{n+2}+e^n+\phi(t_{n+2})+\phi(t_n)|,\nabla|e^{n+2}-e^n|) \\ & \lesssim\delta t^2(\|\triangle e^{n+2}\|^2+\|\triangle e^n\|^2)+\delta t^6+\tfrac{1}{4}\|e^{n+2}-e^n\|^2. \end{aligned} \tag{2.22}$$

For the last term, we have

$$2\delta t(R^{n+1},e^{n+2}-e^n)\lesssim\delta t^2\|R^{n+1}\|^2+\frac{1}{4}\|e^{n+2}-e^n\|^2. \tag{2.23}$$

By combining the above estimates, we obtain

$$\begin{aligned} \|\Delta e^{n+2}\|^2 \quad & -\|\Delta e^n\|^2+\gamma\Big(\|\nabla e^{n+2}\|^2-\|\nabla e^n\|^2\Big) \\ & \lesssim\delta t(\|\Delta e^{n+2}\|^2+\|\Delta e^n\|^2+\|\nabla e^{n+2}\|^2+\|\nabla e^n\|^2+\|R^{n+1}\|^2). \end{aligned} \tag{2.24}$$

Summing up the above inequality from $n=0$ to $m\leq[\frac{T}{\delta t}]-1$, using Lemma 2.1 and dropping some unnecessary terms, we obtain

$$\|\Delta e^{m+1}\|^2+\gamma\|\nabla e^{m+1}\|^2\lesssim\delta t\sum_{n=0}^{m}(\|\Delta e^{n+1}\|^2+\gamma\|\nabla e^{n+1}\|^2)+\delta t^4. \tag{2.25}$$

For the first step ϕ^1, we can use similar analysis and obtain

$$\|\Delta e^1\|^2+\gamma\|\nabla e^1\|^2\lesssim(\delta t_1)^2\lesssim\delta t^4. \tag{2.26}$$

Thus, the induction can start.

By applying the discrete Gronwall Lemma to the inequality (2.25), we have

$$\|\Delta e^{m+1}\|^2+\gamma\|\nabla e^{m+1}\|^2\lesssim\delta t^4, \tag{2.27}$$

which concludes the theorem.

□

2.3 Fourier pseudospectral discretization in space

Since the periodic boundary condition is considered in this paper, it is nature to employ the Fourier pseudospectral method for spatial discretization. Let N_x, N_y be two positive even integers. The spatial domain $\Omega = [0, L_x] \times [0, L_y]$ is uniformly partitioned with mesh size $h_x = L_x / N_x, h_y = L_y / N_y$ and

$$\Omega_h = \{(x_j, y_k) | x_j = jh_x, y_k = kh_y,\ 0 \le j \le N_x - 1, 0 \le k \le N_y - 1\}.$$

Let $V_h = \{u | u = \{u_{j,k} | (x_j, y_k) \in \Omega_h\}\}$ be the space of grid functions on Ω_h. For any two matrix grid functions $\mathbf{F}, \mathbf{G}$ $(\mathbf{F}_{m,n}, \mathbf{G}_{m,n} \in V_h)$, define the discrete inner product and norm as follows

$$(\mathbf{F}, \mathbf{G})_h = \sum_{m,n} \sum_{j=0}^{N_x-1} \sum_{k=0}^{N_y-1} (\mathbf{F}_{m,n})_{j,k} (\mathbf{G}_{m,n})_{j,k} h_x h_y, \quad \|\mathbf{F}\|_h = (\mathbf{F}, \mathbf{F})_h^{1/2}.$$

We define

$$S_N = \text{span}\{X_j(x) Y_k(y), j = 0, 1, \ldots, N_x - 1; k = 0, 1, \ldots, N_y - 1\}$$

as the interpolation space, where $X_j(x)$ and $Y_k(y)$ are trigonometric polynomials of degree $N_x/2$ and $N_y/2$, given respectively by

$$X_j(x) = \frac{1}{N_x} \sum_{m=-N_x/2}^{N_x/2} \frac{1}{a_m} e^{im\mu_x (x - x_j)}, \tag{2.28}$$

$$Y_k(y) = \frac{1}{N_y} \sum_{m=-N_y/2}^{N_y/2} \frac{1}{b_m} e^{im\mu_y (y - y_k)}, \tag{2.29}$$

where

$$a_m = \begin{cases} 1, |m| < N_x/2, \\ 2, |m| = N_x/2, \end{cases} \quad b_m = \begin{cases} 1, |m| < N_y/2, \\ 2, |m| = N_y/2, \end{cases}$$

and $\mu_x = 2\pi / L_x, \mu_y = 2\pi / L_y$. We define the interpolation operator $I_N : C(\Omega) \to S_N$ as follows:

$$I_N u(x, y) = \sum_{j=0}^{N_x-1} \sum_{k=0}^{N_y-1} u_{j,k} X_j(x) Y_k(y), \tag{2.30}$$

where $u_{j,k} = u(x_j, y_k)$.

To obtain derivative $\partial_x^{s_1} \partial_y^{s_2} I_N u(x, y)$ at collocation points, we differentiate (2.30) and

evaluate the resulting expressions at point (x_j,y_k):

$$\partial_x^{s_1}\partial_y^{s_2} I_N u(x_j,y_k) = \sum_{m_1=0}^{N_x-1}\sum_{m_2=0}^{N_y-1} u_{m_1,m_2}(\mathbf{D}_{s_1}^x)_{j,m_1}(\mathbf{D}_{s_2}^y)_{k,m_2},$$

where $\mathbf{D}_{s_1}^x$ and $\mathbf{D}_{s_2}^y$ are $N_x\times N_x$, $N_y\times N_y$ matrices, respectively, with elements given by

$$(\mathbf{D}_{s_1}^x)_{j,m} = \frac{d^{s_1}X_m(x_j)}{dx^{s_1}},\ (\mathbf{D}_{s_2}^y)_{k,m} = \frac{d^{s_2}Y_m(y_k)}{dy^{s_2}}.$$

Define two operators ⓧ and ⓨ as follows:

$$(\mathbf{A}ⓧu)_{j,k} = \sum_{m=0}^{N_x-1}\mathbf{A}_{j,m}u_{m,k},$$
$$(\mathbf{B}ⓨu)_{j,k} = \sum_{m=0}^{N_y-1}\mathbf{B}_{k,m}u_{j,m},$$

where $u\in V_h$. It is easy to show that the two operators possess the following properties:

$$\begin{aligned}\mathbf{A}ⓧ\mathbf{B}ⓨu &= \mathbf{B}ⓨ\mathbf{A}ⓧu,\\ \mathbf{A}ⓐ\mathbf{B}ⓐu &= (\mathbf{AB})ⓐu,\ ⓐ = ⓧ \text{ or } ⓨ.\end{aligned}$$

Then we have

$$\partial_x^{s_1}\partial_y^{s_2}u(x_j,y_k) = (\mathbf{D}_{s_1}^xⓧ\mathbf{D}_{s_2}^yⓨu)_{j,k}.$$

Lemma 2.3 ([12]). *Denote*

$$\mathbf{\Lambda}_{\alpha,s} = \begin{cases} i\mu_\alpha \mathrm{diag}\Big(0,1,\ldots,\frac{N_\alpha}{2}-1,0,-\frac{N_\alpha}{2}+1,\ldots,-1\Big), \text{ when } s \text{ odd},\\ i\mu_\alpha \mathrm{diag}\Big(0,1,\ldots,\frac{N_\alpha}{2}-1,\frac{N_\alpha}{2},-\frac{N_\alpha}{2}+1,\ldots,-1\Big), \text{ when } s \text{ even},\end{cases} \quad \alpha = x \text{ or } y,$$

we have

$$\mathbf{D}_s^\alpha = F_{N_\alpha}^{-1}\mathbf{\Lambda}_{\alpha,s}^s F_{N_\alpha}, \tag{2.31}$$

where F_{N_α} is the discrete Fourier transform, and $F_{N_\alpha}^{-1}$ is the discrete inverse Fourier transform.

Remark 2.3. With the help of (2.31), we can evaluate the derivatives by using the FFT algorithm instead of the spectral differentiation matrix.

Remark 2.4. If s is odd, $\mathbf{D}_s^\alpha$ is a real antisymmetric matrix; if s is even, $\mathbf{D}_s^\alpha$ is a real symmetric matrix.

In order to derive the algorithm conveniently, we define discrete gradient operators

and the discrete Laplace operator as follows

$$\nabla_h = \begin{pmatrix} \mathbf{D}_1^x ⊛ \\ \mathbf{D}_1^y ⓨ \end{pmatrix},$$

$$\Delta_h = \nabla_h \cdot \nabla_h = (\mathbf{D}_1^x)^2 ⊛ + (\mathbf{D}_1^y)^2 ⓨ.$$

Applying the Fourier pseudospectral method in space to the system (2.5), we obtain the following fully discrete scheme:

Scheme 2.2. *Give the initial condition $\phi^0 = \phi_0 \in V_h$. After we obtained $\phi^n, \phi^{n+1} \in V_h$, we update $\phi^{n+2} \in V_h$ via*

$$\begin{aligned} \frac{\phi^{n+2}-\phi^n}{2\delta t} &= -M\Bigg(\varepsilon^2 \Delta_h^2 \frac{\phi^{n+2}+\phi^n}{2} - \nabla_h \cdot \Big(|\nabla_h \phi^{n+1}|^2 \nabla_h \frac{\phi^{n+2}+\phi^n}{2}\Big) \\ &\qquad -\gamma \Delta_h \frac{\phi^{n+2}+\phi^n}{2} + (1+\gamma)\Delta_h \phi^{n+1}\Bigg), \end{aligned} \tag{2.32}$$

where $\gamma \geq 0$.

Next we present some useful results and prove that Scheme 2.2 possesses the discrete mass conservation and energy dissipation laws.

Lemma 2.4. *For real matrix $\mathbf{A} \in \mathbb{R}_{N_a \times N_a}$, $a = x$ or y, and $u, v \in \mathbb{V}_h$,*

$$(\mathbf{A} ⓐ u, v)_h = (u, \mathbf{A}^T ⓐ v)_h. \tag{2.33}$$

Using anti-symmetry of $\mathbf{D}_1^a$ ($a = x$ or y) and the identity (2.33), we obtain the following discrete integration-by-parts formulae:

$$(f, \mathbf{D}_1^a ⓐ g)_h + (\mathbf{D}_1^a ⓐ f, g)_h = 0, \tag{2.34}$$

and

$$(f, \nabla_h \cdot \mathbf{v})_h + (\nabla_h f, \mathbf{v})_h = 0. \tag{2.35}$$

Due to the discrete integration-by-parts formula (2.35), we have the following theorem.

Theorem 2.5. *Scheme 2.2 conserves the discrete mass conservation law*

$$(\phi^n, 1)_h = (\phi^0, 1)_h, \tag{2.36}$$

and the following discrete energy dissipation law

$$\frac{E_h[\phi^{n+1}, \phi^{n+2}] - E_h[\phi^n, \phi^{n+1}]}{\delta t} = -\frac{1}{M} \left\| \frac{\phi^{n+2}-\phi^n}{2\delta t} \right\|_h^2, \quad \forall n \geq 0, \tag{2.37}$$

where

$$\begin{aligned} E_h[\phi^n,\phi^{n+1}] &= \frac{\varepsilon^2}{4}(\|\Delta_h\phi^n\|_h^2+\|\Delta_h\phi^{n+1}\|_h^2)+\frac{1}{4}(|\nabla_h\phi^n|^2,|\nabla_h\phi^{n+1}|^2)_h \\ &\quad +\frac{\gamma}{4}(\|\nabla_h\phi^n\|_h^2+\|\nabla_h\phi^{n+1}\|_h^2)-\frac{1+\gamma}{2}(\nabla_h\phi^n,\nabla_h\phi^{n+1})_h+(\frac{1}{4},1)_h. \end{aligned}$$

Proof. The proof for the fully discrete case is analogous to that of Theorems 2.1-2.3 and thus is omitted. □

3 Numerical Results

In this section, we will give several numerical simulations of the MBE model by the Scheme 2.2. The efficiency and accuracy of the proposed numerical scheme will be demonstrated as well. We choose periodic boundary conditions on the square domain $[0,L]^2$ in this paper. Define the roughness measure function $W(t)$ as follows:

$$W(t)=\sqrt{\frac{1}{|\Omega|}\int_\Omega\Big(\phi(x,y,t)-\overline{\phi}(x,y,t)\Big)^2 d\Omega}, \tag{3.1}$$

where $\overline{\phi}(x,y,t)=\int_\Omega\phi(x,y,t)d\Omega$.

3.1 Accuracy Test

Consider the MBE model (2.1) with the initial condition

$$\phi(x,y,t=0)=0.1(\sin 3x\sin 2y+\sin 5x\sin 5y). \tag{3.2}$$

We take the computational domain as $[0,2\pi]^2$. Furthermore, the space is discretized by 128×128 grid points.

Firstly, we begin with time accuracy test for the Scheme 2.2. We use numerical results of Scheme 2.2 with $\gamma=0$, $\delta t=2\times 10^{-5}$ and $N=128$ as the exact solution since the exact solution for MBE growth model is unknown. We take $\varepsilon=1$ and compute the numerical errors at $t=1$. Table 3.1 lists the L^2-errors versus time step δt for the MBE growth model using the Scheme 2.2 with γ=0,1,2,5. We can observe that the expected second order convergence rate in time is obtained with different stabilized parameter γ. Also we conclude that the accuracy will be improved by adding the stabilized term.

Table 3.1: Error and convergence rate

	$\gamma=0.0$		$\gamma=1.0$		$\gamma=2.0$		$\gamma=5.0$	
Δt	L^2-error	Order	L^2-error	Order	L^2-error	Order	L^2-error	Order
8.0×10^{-4}	2.039e-08	–	1.826e-08	–	1.862e-08	–	1.983e-08	–
4.0×10^{-4}	5.657e-09	1.850	4.598e-09	1.971	4.677e-09	1.993	4.988e-09	1.991
2.0×10^{-4}	1.588e-09	1.832	1.149e-09	2.064	1.163e-09	2.006	1.202e-09	2.007
1.0×10^{-4}	3.907e-10	2.023	2.833e-10	1.999	2.845e-09	2.032	3.031e-09	2.033

3.2 Example 1

Here we present a classical example by using the initial condition (3.2) and choosing $\varepsilon^2=0.1$. In Figure 3.1, we show the contour lines of the numerical solutions ϕ up to the steady state $(t=30)$ by Scheme 2.2. The transient dynamics agrees qualitatively well with those in published literatures, for instance [22,32,35].

In addition, the evolution of energy curves and the roughness are plotted in Figure 3.2 and Figure 3.3, respectively. We observe four transitions in the energy curve and roughness curve corresponding to results in Figure 3.1. These also agree quantitatively well with those in literature.

At the same time, we give the time evolution of the energy when $t\in[0,15]$ with different time step δt and stabilizer γ, shown in Figure 3.4. Also, we enlarge time evolution of the energy with different time step and γ at time region $[0,0.012]$ (left) and $[4,12]$ (right) respectively (shown in Figure 3.5), since the energy are decaying rapidly between this two time intervals. From Figure 3.5, we observe the energy evolution is very close to the exact one with time step $\delta t=10^{-4}$, and $\delta t=10^{-3}$ by adding stabilizer $\gamma=1.0$. But the results with $\delta t=10^{-3}$ without adding stabilizer γ is not accurate enough. Therefore, the stabilizer γ is crucial to the accuracy of the energy evolution.

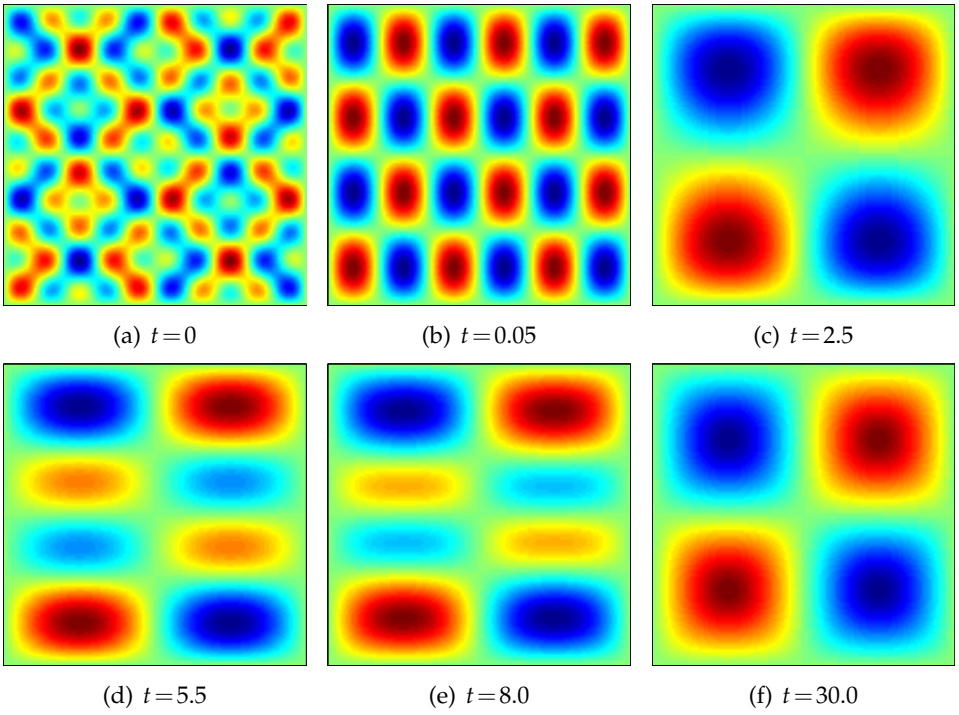

(a) $t=0$ (b) $t=0.05$ (c) $t=2.5$

(d) $t=5.5$ (e) $t=8.0$ (f) $t=30.0$

Figure 3.1: The isolines of numerical solutions of the height function ϕ for the MBE growth model. With $\varepsilon^2=0.1, \gamma=20$ and time step $\delta t=0.001$. Snapshots are taken at $t=0,0.05,2.5,5.5,8,30$, respectively.

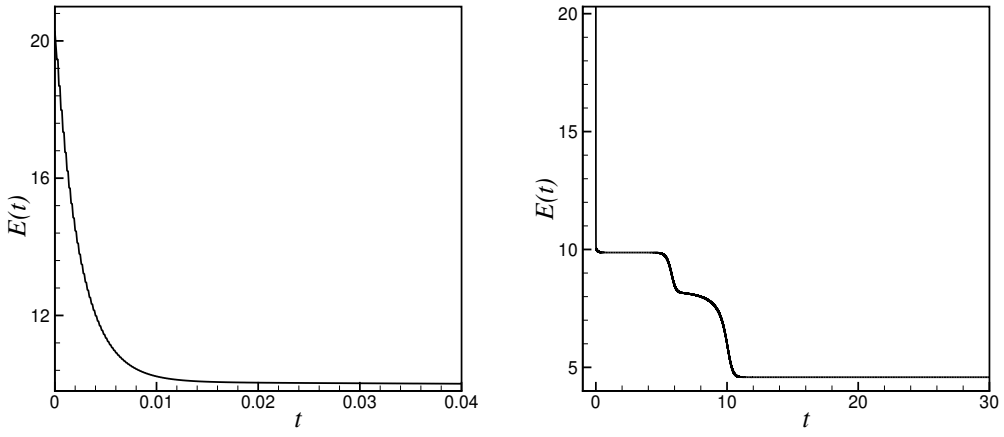

Figure 3.2: Time evolution of the energy for the MBE growth model when $t\in[0,30]$. The time step is set at $\delta t=10^{-3}$ and $\gamma=0$.

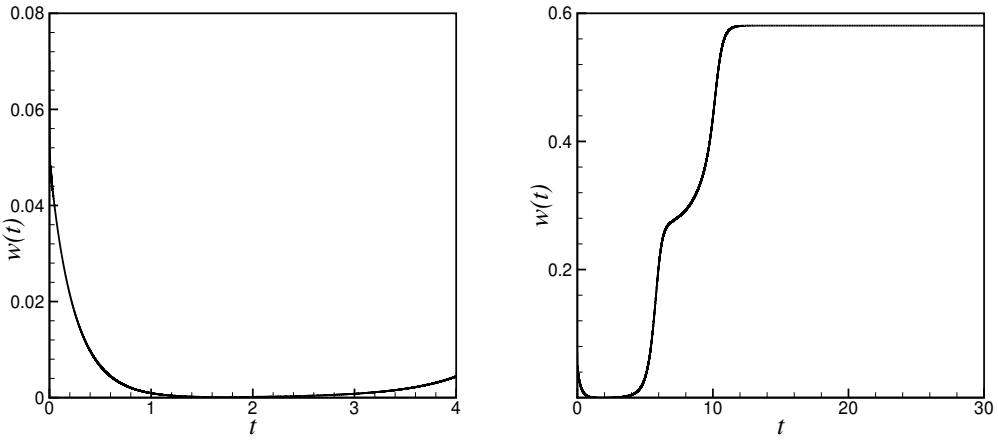

Figure 3.3: Time evolution of the roughness for the MBE growth model. The time step is set at $\delta t = 10^{-3}$ and $\gamma = 0$.

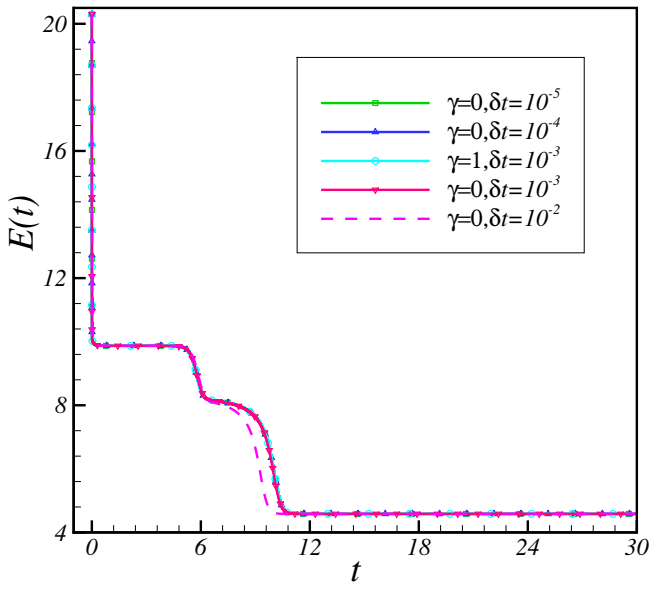

Figure 3.4: Time evolution of the energy for the MBE growth model using scheme (2.2) when $t \in [0,15]$ with different time step and γ.

3.3 Example 2

In this example, we perform numerical simulations of coarsening dynamics in the domain $[0, L]^2$ with $L = 12.8$ and $\varepsilon = 0.03$. The initial condition is a random state by assigning a random number which varies from -0.001 to 0.001 to each grid points.

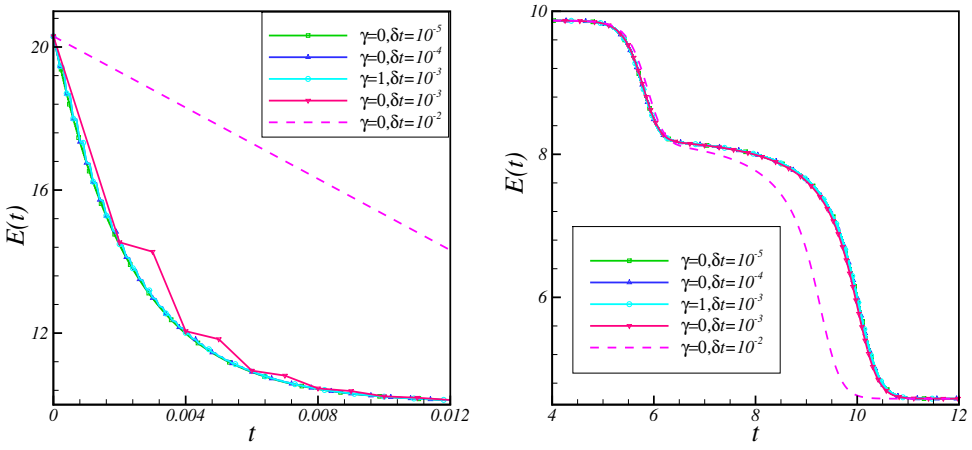

Figure 3.5: Enlarge time evolution of the energy for the MBE growth model with different time step and γ at time region [0, 0.012] (left) and [4,12] (right) respectively.

Table 3.2: δt_c with different γ for the MBE growth model using Scheme 2.2.

γ	0.0	1.0	2.0	3.0
δt_c	$0.003 < \delta t_c < 0.004$	$0.01 < \delta t_c < 0.02$	$0.1 < \delta t_c < 0.2$	$\delta t_c > 1$

Define δt_c as the largest possible time step which allows stable numerical computation. In Table 3.2, we list the values of δt_c for the MBE growth model using Scheme 2.2 with different stabilized parameter γ. The semi-discrete Scheme 2.1 is approximated by the Fourier spectral methods in space with Fourier mode number $N = 512$. Table 3.2 demonstrate that the improvement on stability with the use of γ is significant and the scheme is unconditional stable when γ is sufficiently large.

In Figure 3.6, we plot the time evolution of the energy (left) and roughness (right) with random number condition when $t \in [0.1, 100]$ respectively. We observe that the energy decrease approximately like $t^{-\frac{1}{3}}$ and the growth rate of the roughness function is $t^{\frac{1}{3}}$.

The contour lines of numerical solutions of the height function ϕ and its Laplacian $\Delta\phi$ for the MBE growth model with random initial condition are shown in Figure 3.7. The time step is $\delta t = 0.0001$. Snapshots are taken at $t = 0,1,10,50,100,500$, respectively.

Acknowledgments

Lizhen Chen would like to acknowledge the support from National Science Foundation of China through Grant 11671166 and U1530401 , Postdoctoral Science Foundation of China through Grant 2015M580038. Jia Zhao's work is partially supported by a startup fund, and a seed grant (Research Catalyst Grant) from Office of Research and Gradu-

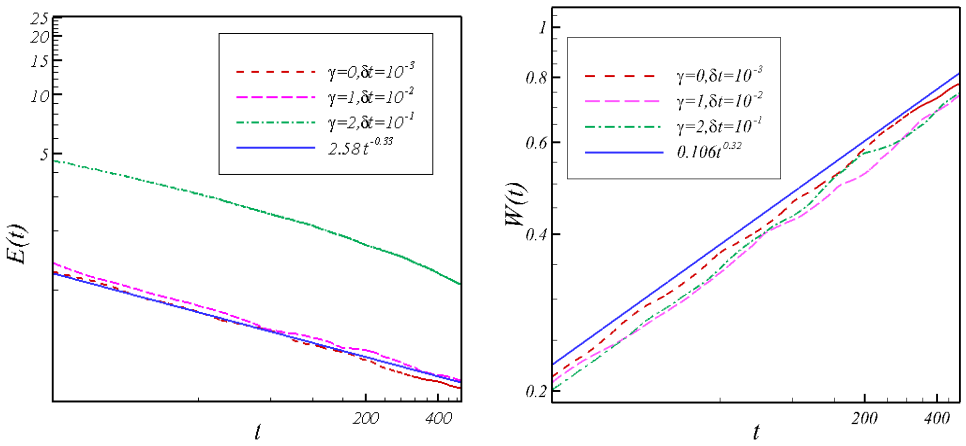

Figure 3.6: Time evolution of the energy (left) and roughness (right) for the MBE growth model with random number condition when $t \in [0.1,100]$ respectively.

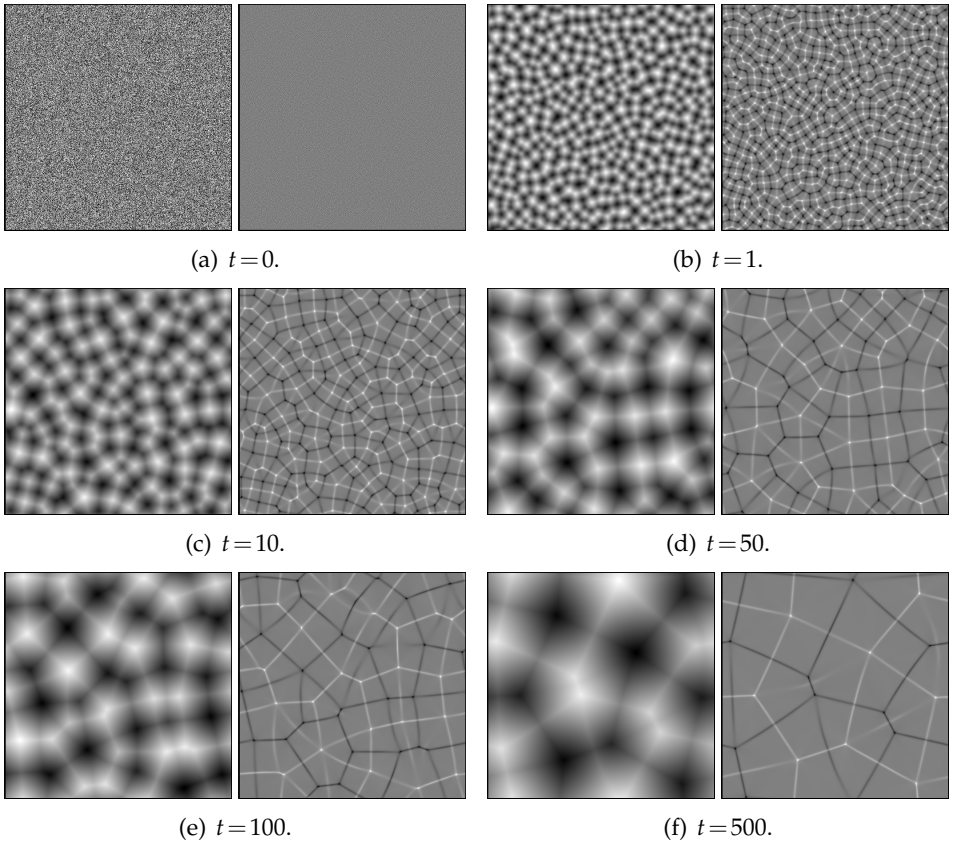

(a) $t=0$. (b) $t=1$.

(c) $t=10$. (d) $t=50$.

(e) $t=100$. (f) $t=500$.

Figure 3.7: The isolines of the height function ϕ and its Laplacian $\Delta\phi$ for the MBE growth model with random initial condition. The time step is $\delta t=0.0001$. Snapshots are taken at $t=0,1,10,50,100,500$, respectively.

ate Studies at Utah State University. Yuezheng Gong's work is partially supported by China Postdoctoral Science Foundation through Grants 2016M591054 and the foundation of Jiangsu Key Laboratory for Numerical Simulation of Large Scale Complex Systems (201703).

References

[1] R. E. Caflisch, M. F. Gyure, B. Merriman, S. Osher, C. Ratsch, D. D. Vvedensky and J. J. Zinck, Island dynamics and the level set method for epitaxial growth, Appl. Math. Lett., 12(1999),13–22.
[2] L. Chen, J. Zhao and X. Yang, Regularized linear schemes for the molecular beam epitaxy model with slope selection, Appl. Numer. Math., 128(2018), 139–156.
[3] W. Chen, C. Wang, X. Wang and S. M. Wise, A linear iteration algorithm for a second-order energy stable scheme for a thin film model without slope selection, J. Sci. Comput., 59(2014),574–601.
[4] W. Chen and Y. Wang, A mixed finite element method for thin film epitaxy, Numer. Math., 122(2012),771–793.
[5] Y. Cheng, A. Kurganov, Z. Qu and T. Tang, Fast and stable explicit operator splitting methods for phase-field models, J. Comput. Phys., 303(2015),45–65.
[6] S. Clarke and D. D. Vvedensky, Origin of reflection high-energy electron-diffraction intensity oscillations during molecular-beam epitaxy: A computational modeling approach, Phys. Rev. Lett., 58(1987), 2235–2238.
[7] M Dahlby and B Owren, A general framework for deriving integral preserving numerical methods for pdes, SIAM J. Sci. Comput., 33(2011), 2318–2340.
[8] D. Eyre, Unconditionally gradient stable time marching the Cahn-Hilliard equation, Computational and mathematical models of microstructural evolution, 529(1998), 39–46.
[9] W. Feng, C. Wang, and S. Wise, Linearly preconditioned nonlinear conjugate gradeint solvers for the epitaxial thin film equation with slope selection, arXiv, (2017), 1–15.
[10] W. Feng, C. Wang, S. Wise and Z. Zhang, A second-order energy stable backward differentiation formula method for the epitaxial thin film equation with slope selection, ArXiv:1706.01943, (2017).
[11] L. Golubovic, Interfacial coarsening in epitaxial growth models without slope selection, Physical Review Letters, 78(1997), 90–93.
[12] Y. Gong, J.X. Cai and Y.S. Wang, Multi-symplectic Fourier pseudospectral method for the Kawahara equation, Commun. Comput. Phys, 16(2014), 35–55.
[13] Y. Gong, J. Zhao and Q. Wang, An energy stable algorithm for a quasi-incompressible hydrodynamic phase-field model of viscous fluid mixtures with variable densities and viscosities, Computer Physics Communications, 219(2017), 20–34.
[14] Y. Gong, J. Zhao, X. Yang and Q. Wang, Second-order linear schemes for hydrodynamic phase field models of viscous fluid flows with variable densities, SIAM J. Sci. Comput., 40(2017), 138–167.
[15] M. F. Gyure, C. Ratsch, B. Merriman, R. E. Caflisch, S. Osher, J. J. Zinck and D. D. Vvedensky, Level-set methods for the simulation of epitaxial phenomena, Phys. Rev. E, 58(1998), 6927–6930.
[16] L. Ju, X. Li, Z. Qiao and H. Zhang, Energy stability and error estimates of exponential time differencing schemes for the epitaxial growth model without slope selection, Math. Com-

put., 87(2017), 1859-1885.
[17] H. C. Kang and W. H. Weinberg, Dynamic monte carlo with a proper energy barrier: Surface diffusion and two-dimensional domain ordering, J. Chem. Phys., 90(1989), 2824–2830.
[18] R. V. Kohn and X. Yan, Upper bound on the coarsening rate for an epitaxial growth model, Comm. Pure Appl. Math., 56(2003), 1549–1564.
[19] J. Krug, Origins of scale invariance in growth processes, Adv. in Phys., 46(1997), 139–282.
[20] H. Lee, J. Shin and J. Lee, A second-order operator splitting fourier spectral method for models of epitaxial thin film growth, J. Sci. Comput., 71(2017), 1303-C1318.
[21] B. Li and J. Liu, Epitaxial growth without slope selection: energetics, coarsening and dynamic scaling, Journal of Nonlinear Science, 14(2004), 429–451.
[22] B. Li and J. G. Liu, Thin film epitaxy with or without slope selection, European Journal of Applied Mathematics, 14(2003), 713–743.
[23] D. Moldovan and L. Golubovic, Interfacial coarsening dynamics in epitaxial growth with slope selection, Physical Review E, 61(2000), 6190–6214.
[24] Z. Qiao, Z. Sun and Z. Zhang, The stability and convergence of two linearized finite difference schemes for the nonlinear epitaxial growth model, Numerical Methods for Partial Differential Equations, 28(2011), 1893–1915.
[25] Z. Qiao, Z. Sun and Z. Zhang, Stability and convergence of second-order schemes for the nonlinear epitaxial growth model without slope selection, Math. Comp., 84(2015), 653–674.
[26] Z. Qiao, C. Wang, S. Wise and Z. Zhang, Error analysis of a finite difference scheme for the epitaxial thin film model with slope selection with an improved convergence constant, International Journal of Numerical Analysis and Modeling, 14(2017), 1–23.
[27] Z. Qiao, Z. Zhang and Tao Tang, An adaptive time-stepping strategy for the molecular beam epitaxy models, SIAM J. Sci. Comput., 33(2011), 1395–1414.
[28] M. Schneider, I. K. Schuller and A. Rahman, Epitaxial growth of silicon: A moleculardynamics simulation, Phys. Rev. B., 46(1987), 1340–1343.
[29] J. Shen, C. Wang, X. Wang and S. Wise, Second-order convex splitting schemes for gradient flows with Ehrlich-Schwoebel type energy: application to thin film epitaxy, SIAM Journal of Numerical Analysis, 50(2012), 105–125.
[30] J. Shen, J. Xu and J. Yang, A new class of efficient and robust energy stable schemes for gradient flows, ArXiv:1710.01331, (2017).
[31] J. Villain, Continuum models of critical growth from atomic beams with and without desorption, J. Phys. I, 3(1991), 19–24.
[32] C. Wang, X. Wang and S. Wise, Unconditionally stable schemes for equations of thin film epitaxy, Discrete and Continuous Dynamic Systems, 28(2010), 405–423.
[33] C. Wang, X. Wang and S. M. Wise, Unconditionally stable schemes for equations of thin film epitaxy., Discrete and Continuous Dynamic Systems, 28(2010), 405–423.
[34] C. Xu and T. Tang, Stability analysis of large time-stepping methods for epitaxial growth models, SIAM Journal of Numerical Analysis, 44(2006), 1759–1779.
[35] X. Yang, J. Zhao and Q. Wang, Numerical approximations for the molecular beam epitaxial growth model based on the invariant energy quadratization method. J. Comput. Phys., 333(2017), 102–127.
[36] J. Zhao, X. Yang, J. Li and Q. Wang, Energy stable numerical schemes for a hydrodynamic model of nematic liquid crystals, SIAM J. Sci. Comput., 38(2016), 3264–3290.
[37] J. Zhao, X. Yang, J. Shen and Q. Wang, A decoupled energy stable scheme for a hydrodynamic phase field model of mixtures of nematic liquid crystals and viscous fluids, J. Comput. Phys., 305(2016), 539–556.